Article

Development of pH-Responsive Nano Drug Delivery System for Efficient Loading and Release of Hydrophobic Anticancer Drugs

Munibah Qureshi and Adeeb Shehzad *

Posted Date: 23 November 2023

doi: 10.20944/preprints202311.1492.v1

Keywords: Drug delivery; Hydrophobic drug; Camptothecin; Mesoporous Silica Nanoparticles

Article

Development of pH-Responsive Nano Drug Delivery System for Efficient Loading and Release of Hydrophobic Anticancer Drugs

Munibah Qureshi and Adeeb Shehzad *

Department of Biomedical Engineering and Sciences, SMME, National University of Sciences and Technology, H-12 Islamabad, Pakistan; munibah.qureshi@smme.nust.edu.pk

* Correspondence: adeeb.shehzad@smme.nust.edu.pk; Tel.: +92-51-90856061

Abstract: The practical application of a pH-responsive Nanoparticle Drug Delivery System (NDDS) in cancer treatment is often hampered by several issues such as the protection of therapeutic molecules from external stresses, inefficient targeted delivery, sustained drug release, and poor efficacy. This study presents an effective design strategy for the synthesis of a pH-sensitive controlled hydrophobic drug delivery method based on the formulation of chitosan (CS)-coated mesoporous silica nanoparticles (MSNs) through the sol-gel method, where hydrolysis takes place in the acidic medium followed by polycondensation of the hydrolyzed products. For this purpose, NH2 modified-MSNs were prepared by using tetraethyl orthosilicate (TEOS) as precursor and cetyltrimethylammonium bromide (CTAB) as a template, and 3-aminopropyltriethoxysilane (APTES) for amine modification, followed by hydrophobic drug loading and CS coating of various concentrations. Camptothecin (CPT) was used as a model drug. Fabricated monodispersed functionalized nanoparticles had sizes ranging from 200nm to 245nm with an encapsulation efficiency as high as 90%. The highest encapsulation efficiency was found for 1% CS coating, which released 50% drug in 120h at pH 6.4 and 20% at pH 7.4 respectively. These nanoformulations exhibited pH-responsive release patterns of CPT under two different pH values (pH = 7.4 and pH = 6.4). These results contribute to the optimization of NDDS, with potential implications for nanoformulations designed for controlled and sustained drug release particularly to tumors without affecting healthy cells owing to differences in the pH of the tumor microenvironment and the normal physiological environment of cells.

Keywords: drug delivery; hydrophobic drug; camptothecin; mesoporous silica nanoparticles

1. Introduction

Cancer remains a prevalent global public health issue with a high mortality rate due to the ineffectiveness of the currently available chemotherapeutics [1]. Treating cancer with chemotherapy is challenging because of the dose frequency, multidrug resistance, and low specificity of the drugs, which demands the need for novel treatment strategies to enhance therapeutic efficacy [2]. The pursuit of efficient drug delivery systems (DDS) has given rise to the exploration of groundbreaking nanotechnology-based strategies for the enhancement of hydrophobic chemotherapeutics. Among various nanomaterials, mesoporous silica nanoparticles (MSNs) have attracted significant attention because of their modifiable pore size, structure, surface area, and potential for encapsulating and releasing therapeutic agents [3]. Additionally, MSNs are remarkably biocompatible and biodegradable via efficient interaction with the body and interstitial fluids in the cells as well as in the body. Water molecules can degrade mesoporous silica by hydrolyzing and dissolving the silica framework [4]. This process can be accelerated by acidic pH, high temperatures, and large surface area. The degradation of MSN can be reduced by using a higher pH, lower temperature, coating the silica framework, or using a different material [5]. During the degradation of MSN, the silanol groups on the surface of the silica form hydrogen bonds with water molecules. This interaction, along with the ionic exchange between

 doi:10.20944/preprints202311.1492.v1

the silica surface and the surrounding medium, accelerates the degradation process [4,5]. By modifying the pore characteristics and surface of MSNs with gatekeeper molecules, such as organic, inorganic, drug molecules, and biological membranes, it is possible to develop formulations that can release drugs on demand and selectively deliver hydrophobic drugs [6].

Despite advancements in drug delivery systems (DDS), challenges remain in achieving controlled and sustained drug release profiles to maximize therapeutic efficacy. Chitosan (CS) is one of the best coating polymers used extensively in NDDS owing to its biocompatibility, biodegradability, nontoxicity (up to a certain concentration), and muco/bioadhesive properties [7,8]. CS is a polysaccharide and a natural polymer, derived from chitin, found in the exoskeletons of crustaceans and the cell walls of fungi [7]. It forms stable nanoparticles through electrostatic interactions. Its applications in DDS have been broadly explored due to its ability to modulate drug release profiles, enhance cellular uptake, and protect encapsulated drugs from degradation [9]. Numerous studies have been designed to extend its residency by improving the contact with the cell surface, thus increasing absorption and strengthening therapeutic efficacy via local drug delivery.

Camptothecin (CPT) is a potent anticancer alkaloid. It acts as a topoisomerase I inhibitor disrupts DNA replication, and induces apoptosis in cancer cells [10]. However, the clinical efficacy of camptothecin is restricted owing to its hydrophobicity, high toxicity, low specificity, and instability at physiological pH [11]. Thus, CPT was used as a model hydrophobic drug to identify accurate methods to overcome these challenges, thereby, augmenting the therapeutic potential of this promising anticancer agent. Previously, different methods were developed to deliver CPT to tumors, including using micelles, liposomes, polymer conjugates, and nanoparticles [12–14]. Of these, nanoparticles made of polymers are the most popular because they have unique properties. Most polymer drug carriers cannot actively target tumors, but they can passively target tumors through a process called the enhanced permeability and retention effect. This means that the nanoparticles can stay in circulation for an extended time and accumulate in tumors, where they can enter the tumor tissue more easily [2,15,16]. However, there are still several challenges with using passive targeting delivery systems for CPT, such as low concentrations of CPT in the target tissue and unpredictable toxicity [2,17]. Therefore, surface-attached targeting molecules can effectually target cancer cells without affecting normal cells.

This study comprehensively investigates the impact of different CS coatings on CPT-loaded MSNs. By varying the CS concentration, we sought to optimize the drug release profile, ensuring sustained and controlled release of CPT over an extended period. The central objective was to elucidate how CS coating influences the physicochemical properties of these nanoparticles and subsequently affects drug release behavior. The loading efficiency and release profile were confirmed by spectrophotometer. The aforementioned NDDS were characterized by advanced techniques such as SEM, DLS, and BET, and chemical interactions between the CS, CPT, and NPs were studied by FTIR. TGA was used to assess the thermal stability of the nanoparticles. Insights gained from the evaluation of drug release kinetics will contribute to tailoring drug delivery profiles to specific biomedical applications and to the development of more effective and targeted drug delivery systems, ultimately improving therapeutic outcomes for cancer treatment.

2. Materials and methods

Tetraethyl orthosilicate (TEOS, 98%), (3-aminopropyl) triethoxysilane (APTES, ≥98%), cetyltrimethylammonium bromide solution (CTAB, 25 wt.%), ammonium hydroxide and glutaraldehyde solution (25 wt.%) and (S)-(+)-Camptothecin (CPT ≥ 90%), were purchased from Sigma Aldrich. Ethanol (EtOH, HPLC grade), dimethyl sulfoxide (DMSO), hydrochloric acid (HCl, ACS reagent, fuming, 37%), and Glacial acetic acid (< 99%) were obtained from Merck. All reagents and solvents used were of analytical grade. Deionized water was used in all experiments.

2.1. Formulation of functionalized mesoporous silica nanoparticles MSNs

MSNs were synthesized using previously reported methods (sol-gel process) with slight adjustments [18]. Briefly, 250 mg of CTAB was dissolved in 120 mL of DI water, followed by the

 doi:10.20944/preprints202311.1492.v1

addition of 1 mL of 2M NaOH. The solution was heated to 80 °C. Once the temperature reached 80 °C, 1.80ml TEOS and 0.120ml APTES were added corresponding to a molar ratio of 10:1, TEOS: APTES, sonicated, and stirred the resulting solution overnight at 80 °C. The particles were then washed repeatedly at 6000g for 25 min, 3X with ethanol, and 3X with DI water to remove the surfactant until the supernatant became clear and no longer foaming anymore. The NPs were re-dispersed in DI water and lyophilized. Functionalized MSNs were denoted as FMSN and non-functionalized MSNs collected before the APTES modification step were denoted as MSN.

2.2. Drug Loading

FMSN (45mg), were dispersed in 1 ml CPT solution in DMSO as 5%of carrier. To disperse the suspension, it was first sonicated on ice for 2 min and stirred at room temperature for 18h while protecting it from light. The resulting suspension was centrifuged at 10,000× *g* at 4 °C/20 mins/4 times with DI water, re-suspended in a certain amount of DI water, and lyophilized. Drug-loaded NPs were represented as FMSN-CPT.

2.3. Chitosan coating o and Crosslinking to FMSN by glutaraldehyde

FMSNs (45mg) or drug loaded FMSN, dispersed in DMSO. 2ml **1**% glutaraldehyde (GA) was added dropwise to the reaction mixture and allowed to react for 1h followed by dropwise addition of 0.5%,1%, and 1.5% CS percentages (in 1% acetic acid) in each reaction setup after sonication reactions were allowed to stir for particular time points and collected at 8, 16, and 20hrs. The resulting suspensions were then washed by centrifugation at 10000 rpm for 20 minutes/four time times with DI water, re-suspended in a certain amount of DI water, and lyophilized. NPs were denoted as FMSN-GA-CS-8, FMSN-CS-GA-16, and FMSN-CS-GA-20, along with specific percentages of CS.

2.4. Camptothecin (CPT) Quantification

CPT concentration was determined using a UV-3600i Plus UV-Vis-NIR spectrophotometer (λmax (CPT) = 366nm). The drug loading efficiency (DLE) and loading capacity (LC %) were calculated as follows:

$$\text{LE \%} = [\text{mass of loaded drug in carrier/total amount of drug initially used}] \times 100$$

$$\text{LC (wt\%)} = (\text{mass of CPT in MSN @CPT})/(\text{mass of MSN}) \times 100$$

2.5. In vitro release assay

To assess the rate of drug release from 0.5%,1% and 1.5% of CS coated MSNs, a known concentration of CPT (100ul) was filled into Slide-A-Lyzer Mini dialysis unit 10KDa MWCO (ThermoFisher) in triplicates, incubated at 37 °C and allowed to release in 1ml 1X PBS at pH 7.4 and pH 6.5 at gentle shaking. The solution was then replaced with fresh 1x PBS at specific intervals. The CPT concentration in the dialyzed fluid was quantified using a Thermo Scientific Multiskan sky microplate reader.

2.6. Hemolysis Assay

Hemolysis assay was performed according to the method available in the literature [19]. Briefly, fresh human blood was collected in the EDTA tubes followed by centrifugation at 6000 rpm for 10 mins to separate plasma and red blood cells (RBC). The pellet was rinsed 4 times with PBS (7.4) until the supernatant turned clear. RBCs are then diluted ten times with 1XPBS.0.2m of RBCs suspension was then added to 0.8ml of various concentrations of coated and uncoated NPs (1mg/ml, 0.5mg/ml, 0.25mg/ml,0.125mg/ml, 0.0625mg/ml, 0.0312mg/ml). Triton X-100 (2%) was used as a positive control and PBS buffer (pH: 7.4) was taken as a negative control. All the samples were incubated at for 2 hours at 37 °C Afterwards, the incubated samples were centrifuged at 6000 rpm for 10 mins and

 doi:10.20944/preprints202311.1492.v1

supernatant was analyzed at 540 nm by UV spectrophotometer. %Hemolysis was calculated using the formula:

$$\text{Hemolysis\%} = [\text{Abs(sample)} - \text{Abs(Negative Control)}/\text{Abs(positive control} - \text{Abs negative control)}] \times 100$$

2.7. Characterization Techniques

Scanning Electron Microscopy (SEM) equipped with an Energy Dispersive X-ray Microanalysis system (EDX) was employed to examine the surface morphology and size distribution of the nanoparticles. Dynamic Light Scattering (DLS) was used to determine the hydrodynamic diameter and polydispersity of nanoparticles in aqueous suspensions. Brunauer-Emmett-Teller (BET) was used for surface characterization. Fourier-Transform Infrared Spectroscopy (FTIR) was used to study the chemical interactions between the CS, CPT, and NPs. Ultraviolet-visible spectroscopy (UV) analysis was performed to quantify the drug loading efficiency of camptothecin within the nanoparticles. Thermogravimetric Analysis (TGA) was used to assess the thermal stability of the nanoparticles.

2.8. Statistical Analysis

Graphical representation of all of the experiments was carried out using Graph Pad Prism 8 and Origin 2023b. All experiments were done in triplicates. Release experiment groups were compared using one-way ANOVA followed by Tukey's multiple comparisons test for the comparison of three or more groups. The degree of significance is represented as $*p \leq 0.05$ for significant, $**p \leq 0.01$ for very significant, and $***p \leq 0.001$ for highly significant using a 95% confidence interval (p-value ≤0.05).

3. Result and Discussion

3.1. Formulation of NDDS

The MSN nanocarrier was formulated by the Stöber method, using cationic CTAB as a surfactant. Modification by APTES was carried out to confer a positive charge on the NH2 group. Graphical representation of the formulation shown in Figure 1. Because they have amine groups, these positively charged nanocarriers can electrostatically bind to negatively charged molecules like DNA, RNA, drugs, proteins, polysaccharides, and anionic dyes. CPT (negatively charged drug) was then loaded onto a nanocarrier followed by CS coating of various percentages with or without GA, a commonly used crosslinking agent, which reacts with primary amines to form imine (N=C) bond between the aldehyde carbon and primary amines. In a coating of CS without using GA, only a small change was observed in the weight of the end product nanocarrier after washing and drying of NPs. It might be because of the loosely bound CS layer, whereas the use of GA resulted in a more stable and firmly bound layer on the surface of FMSNs, which is in accordance with the previously reported studies [20].

To study how stirring/incubation time affects the concentration of CS coating on FMSN nanoparticles (NPs), NPs were collected at a period of 4 hours, 12 hours, and 18 hours. Then NPs were washed and oven dried at the end of each time point. The weight of the FMSNs before and after, or initial and final, was recorded and calculated to determine the weight gain % of the end product ($\Delta W = (Wf - Wi/Wi \times 100)$. The highest coating percentage was achieved after 18 hours for different concentrations, the point at which almost all of the CS used initially had been consumed. We found the highest weight gain was 60% for 1.5% CS followed by 45% with CS (1%) coating of FMSN at 18h and the lowest at 4% for 0.5% at 4hrs. Weight gain at each time point is shown in Table 1. Thus the percentage of CS coating on the FMSN can be controlled by tuning the conditions of the experiment.

Preprints (www.preprints.org) | NOT PEER-REVIEWED | Posted: 23 November 2023 doi:10.20944/preprints202311.1492.v1

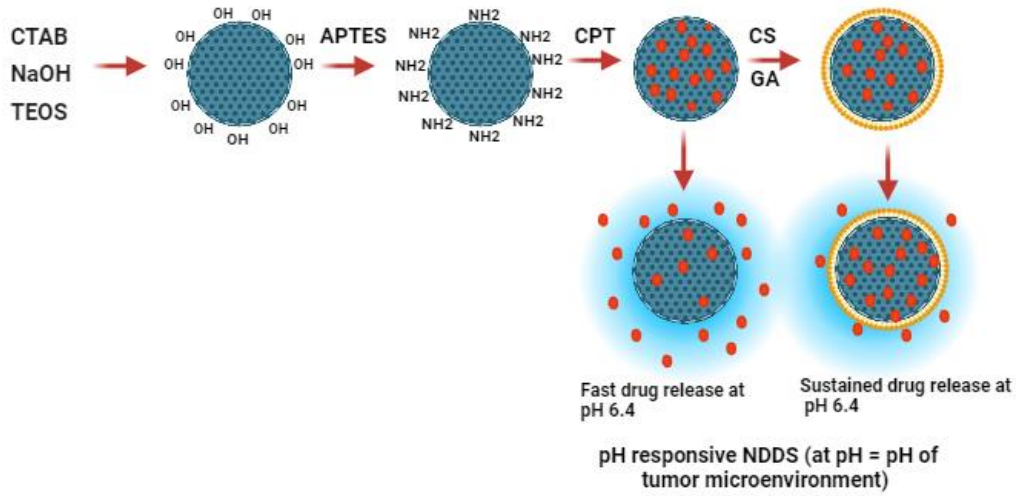

Figure 1. Graphical representation of formulation of MSNS, APTES functionalized MSNs (FMSNs), Camptothecin (CPT) loading, Glutaraldehyde (GA) cross-linking of Chitosan (CS), and drug release at pH 6.4.

Table 1. Effect of stirring time on the coating on FMSN, weight% at each time, calculated using the formula, $\Delta W = Wf - Wi/Wi \times 100$.

CS %	CS Initial (ml)	FMSN (mg)	Final (mg) @ Time points (hr)			Gain (mg) @ Time points (hr)		
			4	12	18	4	2	18
0.5	1	20	20.8	22	24	0.8	2	4
1	1	20	21.5	23	29	1.5	3	9
1.5	1	20	22.8	25	32	2.8	5	12

3.2. Characterization of Functionalized mesoporous silica NPs (FMSN)

The obtained NPs were characterized using DLS, SEM, FTIR, and TGA.

3.2.1. Dynamic light scattering

Dynamic light scattering (DLS) was used to determine the hydrodynamic size, size distribution zeta potential profile of the MSN and FMSN in the solution. As shown in Figure 2, DLS data confirmed that MSN showed a hydrodynamic size of 180nm and zeta potential of -30.7mV due to the dissociation of silanol groups (-Si-OH) on the surface of the NPs. Silanol groups can ionize in aqueous solutions, resulting in the release of hydroxyl ions and leaving behind negatively charged siloxane groups (-Si-O-), which leads to a negative charge on MSN-OH [21]. NH2 modification changed the size to 245 nm and increased the zeta potential to 41mV because of the protonation of the NH2 group. CPT loading to FMSN increased the size to 245nm and reduced the overall charge to 29mV due to the influence of negatively charged CPT molecules (Figure 2B,C). CS coating at different concentrations (0.5%, 1%, and 1.5%) onto FMSNs potentially affected the hydrodynamic size of the NPs due to additional layer on the surface, which increased to a maximum of 343 nm (Figure 2B). Interestingly, 1% CS displayed ideal characteristics, such as optimal size, highly monodispersity, and stability. This may be because 1% concentration may provide sufficient CS molecules to achieve optimal coverage, ensuring a more uniform and complete coating that resulted in improved properties compared to lower or higher concentrations. The zeta potential was not significantly modulated with different concentrations of CS and was found to be around + 44mV, which has been reported previously [20]. Poly disparity index (PDI) of all groups was maintained from 0.4 to 1 while for CS1% coating it was 0.3, which validates the uniformity/monodispersity of prepared NPs (Figure 2A). The change in zeta size and potential at each step suggested successful amino-functionalization, drug loading, and coating of the nanocarrier.

Preprints (www.preprints.org) | NOT PEER-REVIEWED | Posted: 23 November 2023 doi:10.20944/preprints202311.1492.v1

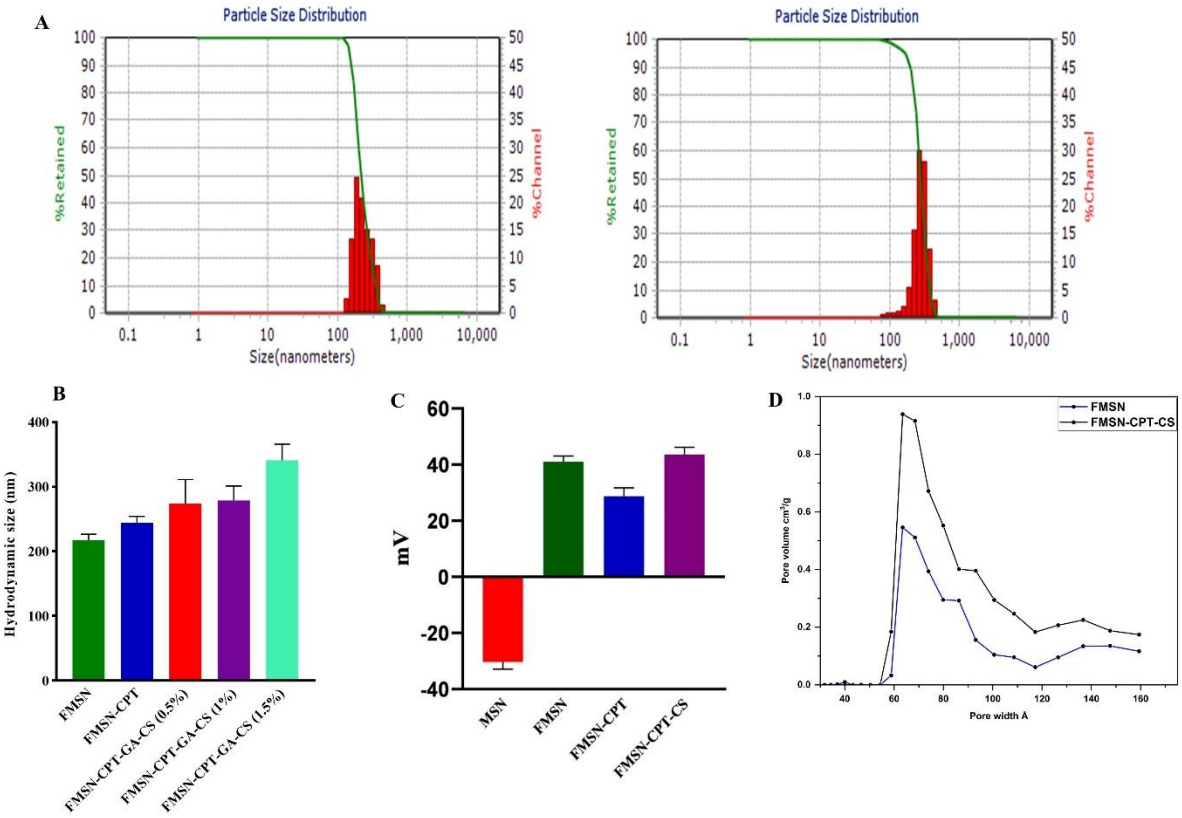

Figure 2. Size distribution of FMSNs and FMSN-CPT-CS (**A**), Hydrodynamic size of NPs (**B**), Zeta potential of NPS (**C**), BJT pore width vs. Pore volume of FMSN and FMSN-CPT-CS (**D**).

3.2.2. Scanning Electron Microscopy

SEM analysis was performed using SEM JSM-6490A by JEOL Japan, to investigate the dry size and surface morphology of the FMSN before and after coating with different concentrations of CS. Approximately 50 NPs were selected and evaluated using ImageJ software. Bare FMSN revealed a uniform and rod-shaped morphology, which can be identified as MCM-41. After coating with 0.5% CS, we observed a change in the surface morphology as well as in the size of the nanoparticles with a 230 nm diameter. The surface became slightly rougher, indicating successful deposition of CS onto the MSN surface (Figure 3B). Increasing the CS concentration to 1% resulted in well segregated and monodispersed NPs but with slight rough edges. At a CS concentration of 1.5%, the SEM images revealed a significant increase in the thickness of the coating by increasing the size to 311 nm of nanoparticles. The nanoparticles appeared to be heavily coated, with a rough and irregular surface and aggregation of particles, indicating the potential influence of the higher CS concentration on the dispersion of the nanoparticles. NP aggregation with increasing concentration has also been reported in other studies [22,23]. The deviation of the SEM results from the DLS study could be attributed to swollen NPs in the hydrodynamic environment, while the former technique represents the dry state of the NPs.

The coating can influence the surface morphology and particle size, with thicker and rougher coatings observed at higher CS concentrations [24–27]. These findings suggest that the CS coating process can be optimized to achieve the desired surface characteristics and dispersion of MSNs for various applications.

Preprints (www.preprints.org) | NOT PEER-REVIEWED | Posted: 23 November 2023 doi:10.20944/preprints202311.1492.v1

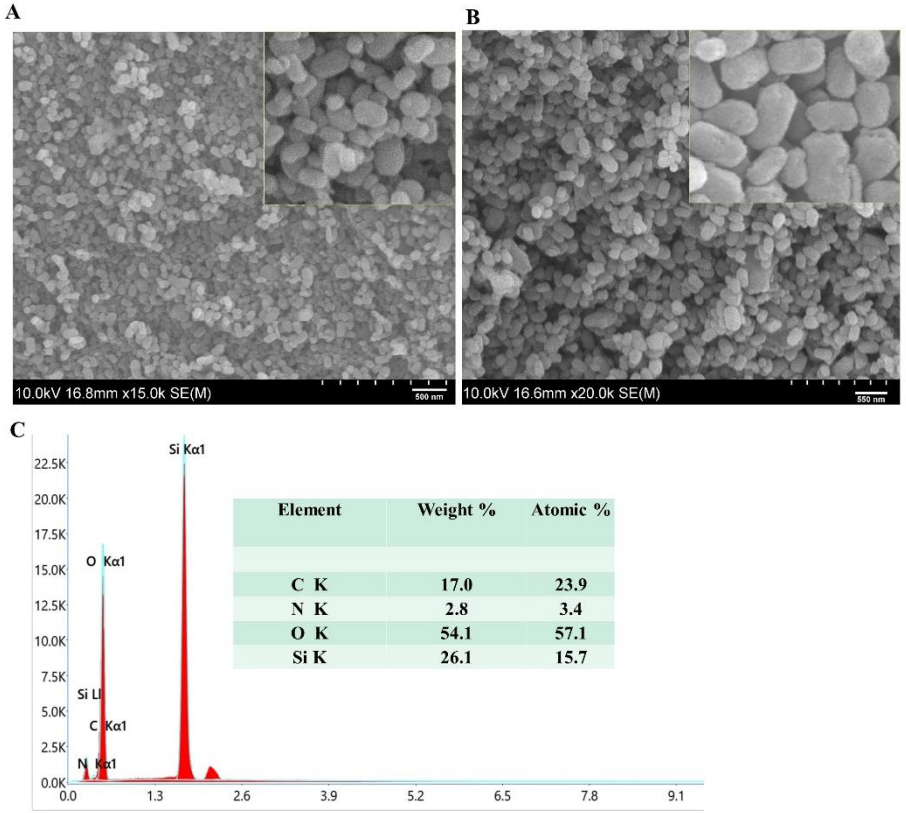

Figure 3. SEM Imgae of FMSN-CPT-CS and (A), Elemental composition of NPs (B).

Table 2. Hydrodynamic size, SEM size, Zeta Potential, and PDI of NPs.

	Zeta size (nm)	SEM size (nm)	Zeta potential (mV)	PDI
FMSN	217	180	+40.32	0.426
FMSN-CPT	245	205	+29.67	0.413
FMSN-CPT-GA-CS (0.5%)	278	230	+44.25	0.663
FMSN-CPT-GA-CS (1%)	282	245	+45.73	0.316
FMSN-CPT-GA-CS (1.5%)	343	311	+44.61	1.625

3.2.3. Fourier-Transform Infrared Spectroscopy

The synthesis of FMSN and the variations in chemical bonding among all groups were investigated using FTIR spectroscopy. As shown in Figure 4A, the absorption peaks of MSN appeared at 945 cm-1,1040 cm-1 and 3200-3600 cm-1.These peaks indicate Si-O-Si asymmetric stretching vibrations and O-H stretching vibrations, which suggest the occurrence of -OH groups or adsorbed water molecules on the surface of the material [28]. NH2 could be confirmed by the stretching vibration of the N-H bond at 3300-3500 cm- 1 bending vibration of the N-H bond in the NH2 group at 1600-1650 cm-1 and stretching vibration of the C-N at 1200-1300 cm-1 [29]. The loading of CPT to FMSN exhibited changes in the intensity and shapes of certain peaks. The spectrum shows peaks that are typical of esters, which are organic compounds that have a carbonyl group (C=O) and a hydroxyl group (-OH). The peak at around 1640 cm-1 is likely due to the stretching of the C=O bond, while the peak at around 3200-3400 cm-1 is likely due to the stretching of the O-H bond. The peaks at around 1600-1500 cm-1 are due to the vibrations of the carbon-carbon double bonds (C=C) in the rings [30,31]. The presence of NH2 groups on the surface of the FMSN allowed for potential interactions with CPT. Our results confirmed that as the percentage of CS coating increased, the intensity of the peaks associated with CS in the spectrum also increased. This suggests that the CS coating was successfully applied to the substrate [32]. The peaks at 3300 to 3500 cm-1 correspond to

Preprints (www.preprints.org) | NOT PEER-REVIEWED | Posted: 23 November 2023 doi:10.20944/preprints202311.1492.v1

the O-H stretching vibrations due to the interaction between the OH groups in CS and FMSN (Figure 4A). This suggests that there is hydrogen bonding between the two materials. The peaks at 1640 cm-1 and 946 to 960 cm-1 correspond to the stretching vibrations of amide bonds (C=O) and the vibration of C-O-C bonds, respectively. These peaks are also characteristic of CS [33]. The bands in the region of 1600-1700 cm-1 indicate the presence of imine bonds (C=N) due to the interaction of GA with the NH2 groups in chitosan (Figure 4A,b,c,d). This suggests that the cross-linking reaction between GA and CS was successful [20]. Overall, the IR spectrum confirms the successful application of a CS coating to the substrate and the cross-linking of the CS coating with GA.

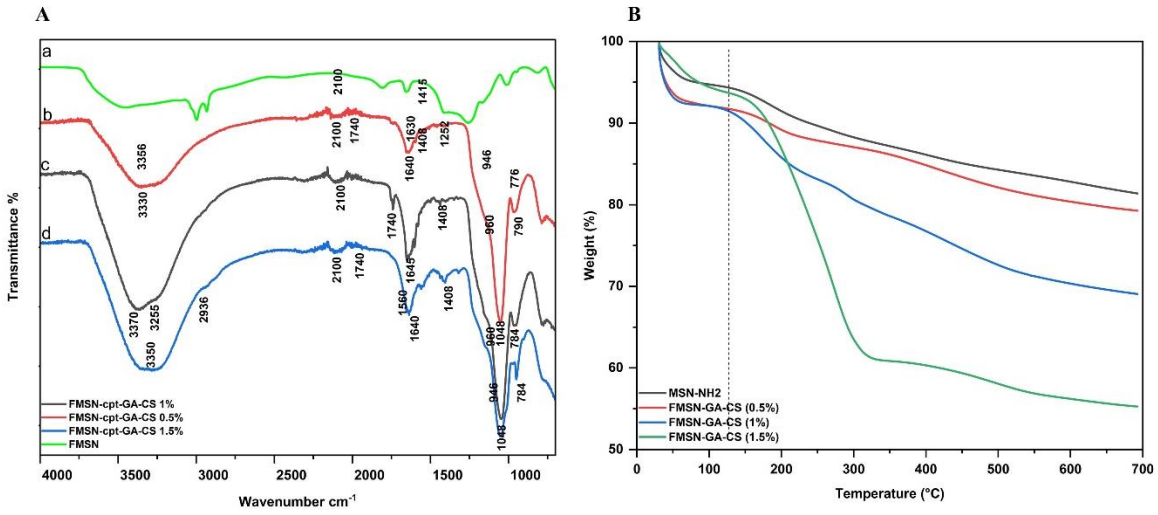

Figure 4. FTIR of formulated NPs (**A**) TGA Thermogram of 0.5%,1%, and 1.5% CS coated FMSNs (**B**).

3.2.4. BET surface analysis

For surface area and pores characterization, BET (Gemini VII 2390 V1.03 (V1.03 t)) was employed in the study. The BET method is a widely used technique for measuring the surface area of a material [34]. In this study, the BET surface area was 712.6392 m^2/g, indicating that the material has a large amount of available surface area for adsorption.The pore size measured using the BET method was 7-13nm, and the pore volume measured by the (Density Functional Theory (DFT) method was 0.45583 cm^3/g (Figure 2D). After the drug loading and CS coating surface area reduced to 415m^2/g while the pore volume decreased to 0.22 cm^3/g as shown in Table 3.

Table 3. Surface characterization of NDDS showing, Surface area, pore volume, and pore size.

	BET surface area (m^2/g)	BET pore volume (cm^3/g)	BJH pore dm (nm)
MSN	712.6392	0.45583	7-13
FMSN-CPT-GA-CS	415m2/g	0.22	-

3.2.5. Thermogravimetric Analysis

The TGA study revealed a two-step weight loss process. The first weight loss was observed below 200 °C due to absorbed water, condensation of silanol groups, and residual solvent evaporation [35].The second weight loss <200 °C could be attributed to the surface functionalization and coated CS, indicating the removal of attached groups from the surface [36,37]. Figure 4B shows the graphs of weight loss (Δw%) as a function of temperature (°C) for the FMSN and CS-coated groups. The higher weight loss (30%) at 210-350 °C could be attributed to the decomposition of CS (OH and NH bonds) in the FMSN-CS (1.5%) sample, compared to the other concentrations, which showed lower Δw% values.

3.3. Drug Loading

The pores of MSN can accommodate both hydrophobic and hydrophilic molecules, making them highly versatile for biomedical and pharmaceutical applications. The anticancer drug CPT is hydrophobic, so DMSO was chosen as the solvent to maximize drug loading. The drug incorporation efficiency of CPT into MSN pores coated with different percentages of CS (0.5%, 1%, and 1.5%) was evaluated. Electrostatic interactions between the positively charged NH2 groups and the reactive sites on CPT resulted in high drug loading and better entrapment efficiency. NH2 functionalization augmented drug loading, which is consistent with many other reports [25,33,38]. FMSNs showed a drug loading (DL) of 4.1% of 5% (0.205%) and an encapsulation efficiency (EE) of 80%, while CS (0.5%)-FMSNs showed a DL of 4.25% and an EE of 85%, CS (1%)-FMSNs showed a DL of 4.5% and an EE of 90%, respectively. CS (1.5%)-FMSNs showed reduced DL because of the presence of a thicker CS coating which reduced the pore size and volume (Figure 2D). This reduction can limit the diffusion and penetration of the drug molecules inside the nanopores, resulting in lower drug loading. The higher viscosity of solutions with higher CS concentrations may be a major factor in the decreased drug loading. It has been reported that high viscosity associated caused by increased CS concentration can make it difficult for drugs to be loaded into nanoparticles [23]. The average yield of nanoparticles was 80 mg/mL, and the maximum drug loading was 4.5% for nanoparticles with a 1% CS coating. This means that 5 mg of nanoparticles could store almost 0.2 mg of CPT.

3.4. Invitro Drug Release Kinetics

An in vitro drug release study was performed to assess the suitability of MSNs as carriers for delivering hydrophobic drugs. The release profile of drugs from NDDS is affected by several factors, including the molecular and chemical properties of the MSN surface, the physicochemical characteristics of the encapsulated drug, and the pH of the release media [39]. Drug release was performed in phosphate-buffered saline (PBS) at pH 7.4 and pH 6.4 at 37 °C, mimicking physiological and tumor microenvironments [40].

The release profile showed an initial burst release during the first 8h of the experiment at both pH values from all groups, likely due to drug adsorption on or around the NP surface [31,39,41]. All of the CPT from the free CPT group was released into the release medium within 24 hours 72% of the drug was released from FMSN-CPT throughout 120 hours. CPT release from FMSN-CPT was not affected, particularly by changes in pH (Figure 5C) whereas significant difference was noted in the drug release patterns from the CS coated groups over 120h (FMSN-CPT-GA-CS (0.5%) released approximately 60% and 28% of its loaded CPT at pH 6.4 and 7.4, respectively (Figure 5D). FMSN-CPT-GA-CS (1%) released 51% and 20% of its loaded CPT at pH 6.4 and 7.4 (Figure 5E), respectively. FMSN-CPT-GA-CS(1.5%) released 28% and 19% of its loaded CPT at pH 6.4 and 7.4, respectively (Figure 5F). The low release percentages from FMSN-CPT-GA-CS (1.5%) were expected because the increased viscosity at higher CS concentrations caused the formation of a denser coating on the nanoparticles after interaction with GA. This resulted in greater crosslink density and less swelling capacity, which reduced drug release [27,33,42]. These release profiles can be explained by the fact that CS-coated FMSNS were significantly influenced by pH, which shows that CS being a pH-sensitive polymer is dependent on the nature of the environment (acidic or neutral) to release the drugs or other therapeutic activities. At pH 7.4, the strong hydrogen bonding between the NH2 groups on the FMSN surface and the nitrogen and oxygen atoms of the encapsulated CPT caused slower drug release. At pH 6.4, the surface NH2 groups of FMSN and OH of CPT were protonated, resulting in repulsive interactions between the positive charges, followed by swelling and pore opening, leading to higher drug release [38,43]. However, it contracted after moving away from the acidic pH, resulting in film formation, which shielded the pores and exhibited a significant reduction in CPT release at higher pH [24]. Thus, as a pH-responsive polymer, CS provided controlled CPT release over time, with an obvious pH-selective release. The rate release is inversely proportional to pH, that is increases with a decrease in pH. Under normal physiological conditions (pH 7.4), negligible CPT release indicates that the NDDS is

Preprints (www.preprints.org) | NOT PEER-REVIEWED | Posted: 23 November 2023 doi:10.20944/preprints202311.1492.v1

well-protected from the drug release in normal tissues, which is essential given the high toxicity of these drugs to healthy cells [44–46]. NPs have been successfully fabricated to direct the drug release exclusively to cancer cells which is highly desirable for targeted anticancer therapy.

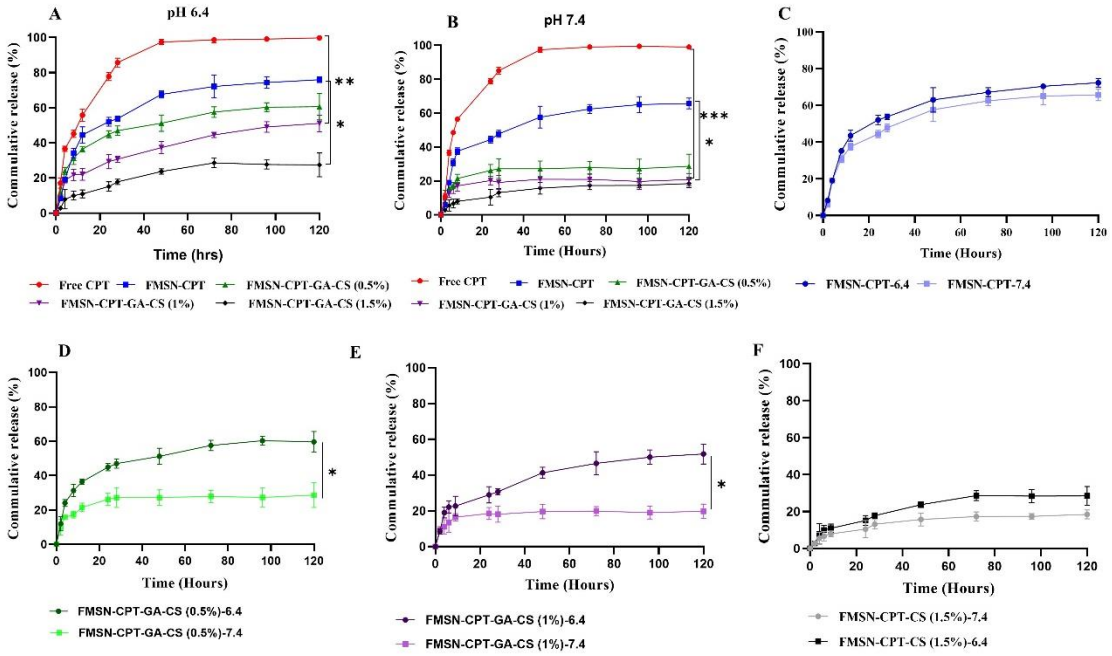

Figure 5. Drug release curves of NDDS, at pH 6.4, pH 6.7 and comparison of each group at pH 7.4 and pH 6.4.

The release kinetics of CPT from CS(1%) coated FMSN were analyzed using various mathematical models as well as shown in Table 4. The R2 values obtained from the zero-order were 0.8288, 0.9894 for the Korsmeyer-Peppas model, and 0.991 for the Weibull model. The R2 values show that the Korsmeyer-Peppas and Weibull models provide good fits to the experimental data, suggesting that CPT release follows anomalous diffusion with a potential Weibull distribution. It can be concluded that more than one mechanism controls the release, considering that surface coating disassembly affects drug-matrix interactions.

Table 4. Drug release kinetics R2 values from three different models.

NDDS	pH	Model		
		0 order	Korsmeyer-Peppas	Weibull models
FMSN	6.4	0.7006	0.9918	0.9950
FMSN-CPT-CS(0.5)	6.4	0.7652	0.9905	0.9930
FMSN-CPT-CS(1)	6.4	0.8288	0.9894	0.9915
FMSN-CPT-CS(1.5)	6.4	0.8026	0.9915	0.9924

4. Hemolysis Assay

It was also important to study the biocompatibility of formulated NPs and the effect of biocompatible coating (CS) on the hemolysis effect of NPs. Visual presentation of the hemolysis effect of FMSN and FMSN-CS is shown in Figure 6D. According to the ASTM E2524-08 standard, only more than 5% hemolysis is considered significant. Results demonstrate that 2% Triton X 100, being positive control caused 100% hemolysis while the negative control 1XPBs displayed almost negligible hemolysis. For NPs, hemolysis has a dose-dependent effect as it increases with increasing concentration. The significant difference in hemolysis percent was found between and coated and

Preprints (www.preprints.org) | NOT PEER-REVIEWED | Posted: 23 November 2023 doi:10.20944/preprints202311.1492.v1

uncoated NPs (p = 0.000187). The highest percent hemolysis (48%) was noted for bare FMSN at a concentration of 1mg/ml decreased at lower concentrations and reached less than 5% at 0.125 mg/ml (Figure 6A). While after CS coating significant decreases in hemolysis was found and less than 5% hemolysis was achieved at 0.5 mg/ml (Figure 6B). The lower concentrations did not show any hemolysis either for FMSN or FMSN-CS (p = 0.8507). Other studies also reported hemolysis by FMSN at the same concentration and found MSNs more toxic [47,48]. This could be explained by the fact that the shielding effect of CS coating on the FMSN surface prevented the hemolysis. It has been reported in the literature that the hemtoxicity of MSNs FMSNs or NPs is dependent on size [49,50]. The particles in nanorange show more toxicity due to the larger surface area that interacts with RBCs to induce hemolysis. Although the coating of NPs prevented the hemolysis as the coating degraded over time, further study is still needed to check the hemolysis effect upon CS coating degradation over time leaving the bare FMSN or MSN surface.

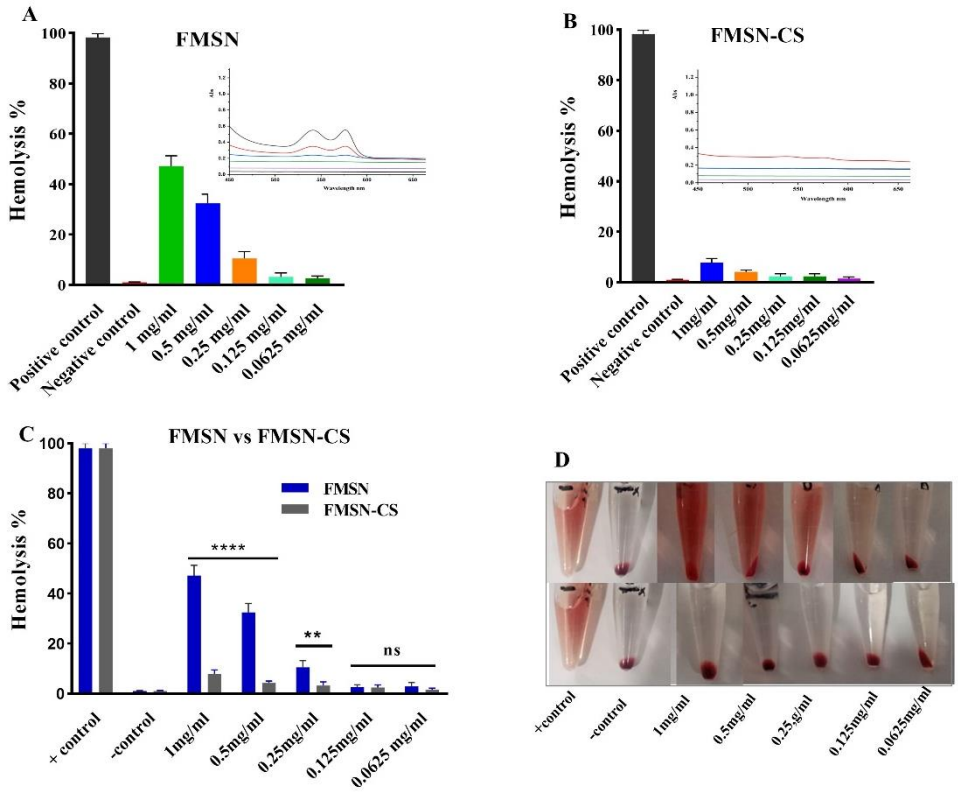

Figure 6. Hemolysis of NPs at various concentrations, FMSN (**A**), FMSN-CS (**B**) NPs p-value < 0.0001 (****) represents significance, p-value >0.05 represents not significant (ns).

5. Conclusion

This study explored the impact of the concentration of natural polymer, and CS coating on the encapsulation and release behavior of hydrophobic drugs on functionalized MSNs. This systematic investigation has shed light on the complex interplay between coating, drug loading, and release kinetics. Our results showed that CS coating concentration significantly influenced the encapsulation efficiency, drug loading capacity, and release kinetics of hydrophobic drugs. A CS coating concentration of 1% was found to be optimal in terms of morphology, physicochemical characteristics, and release behavior. The in vitro drug release studies showed that the release of hydrophobic drugs from all types of carriers was sensitive to the pH of the release medium due to the pH-sensitive coating. The minimum release was observed at pH 7.4, while the maximum release was achieved at pH 6.4, which is a highly desirable approach for drug delivery to inflammatory tissues and tumor cells. Formulated NPs in this study also demonstrated excellent biocompatibility, as proved by the hemolysis assay, they are safe to use at concentrations of

≤0.125mg/ml (FMSN) and ≤0.5mg/ml (FMSN-CS). Therefore, the developed NDDS has significant potential for pharmaceutical formulations designed for controlled and sustained drug delivery to achieve the maximum therapeutic effect for localized drug delivery with minimal adverse effects. Comparing our study with the existing findings, our study contributes to the research efforts supporting the development of biocompatible nanoparticles for drug delivery applications. However, future research should investigate particular aspects, such as long-standing biocompatibility, invitro and in vivo studies and several assays to broadly assess the safety profile of these NPs.

Author Contributions: Conceptualization, M.Q. and A.S.; Methodology, M.Q.; Writing, editing, and review, M.Q. and A.S.; Supervision, A.S. All author has read and agreed to the published version of the manuscript.

Funding: This research received partial funding from the Higher Education Commission (HEC) of Pakistan.

Informed Consent Statement: Not applicable.

Data Availability Statement: Data are contained within the article.

Acknowledgment: We would like to thank Higher Education Commission (HEC) of Pakistan for providing research support in this study.

Conflicts of Interest: The author declares no conflict of interest.

References

1. Siegel, R.L.; Miller, K.D.; Wagle, N.S.; Jemal, A. Cancer Statistics, 2023. *CA. Cancer J. Clin.* **2023**, *73*, 17–48, doi:10.3322/caac.21763.
2. Sun, X.; Zhao, P.; Lin, J.; Chen, K.; Shen, J. Recent Advances in Access to Overcome Cancer Drug Resistance by Nanocarrier Drug Delivery System. *Cancer Drug Resist.* **2023**, *6*, 390–415, doi:10.20517/cdr.2023.16.
3. Isa, E.D.M.; Ahmad, H.; Rahman, M.B.A.; Gill, M.R. Progress in Mesoporous Silica Nanoparticles as Drug Delivery Agents for Cancer Treatment. *Pharmaceutics* **2021**, *13*, 1–33, doi:10.3390/pharmaceutics13020152.
4. Hu, Y.; Bai, S.; Wu, X.; Tan, S.; He, Y. Biodegradability of Mesoporous Silica Nanoparticles. *Ceram. Int.* **2021**, *47*, 31031–31041, doi:10.1016/j.ceramint.2021.08.129.
5. Choi, E.; Kim, S. Surface PH Buffering to Promote Degradation of Mesoporous Silica Nanoparticles under a Physiological Condition. *J. Colloid Interface Sci.* **2019**, *533*, 463–470, doi:10.1016/j.jcis.2018.08.088.
6. Koohi Moftakhari Esfahani, M.; Alavi, S.E.; Cabot, P.J.; Islam, N.; Izake, E.L. Application of Mesoporous Silica Nanoparticles in Cancer Therapy and Delivery of Repurposed Anthelmintics for Cancer Therapy. *Pharmaceutics* **2022**, *14*, doi:10.3390/pharmaceutics14081579.
7. Jafernik, K.; Ładniak, A.; Blicharska, E.; Czarnek, K.; Ekiert, H.; Wiącek, A.E.; Szopa, A. Chitosan-Based Nanoparticles as Effective Drug Delivery Systems—A Review. *Molecules* **2023**, *28*, 1–17, doi:10.3390/molecules28041963.
8. Alizadeh, L.; Alizadeh, E.; Zarebkohan, A.; Ahmadi, E.; Rahmati-Yamchi, M.; Salehi, R. AS1411 Aptamer-Functionalized Chitosan-Silica Nanoparticles for Targeted Delivery of Epigallocatechin Gallate to the SKOV-3 Ovarian Cancer Cell Lines. *J. Nanoparticle Res.* **2020**, *22*, doi:10.1007/s11051-019-4735-7.
9. Sharifi-Rad, J.; Quispe, C.; Butnariu, M.; Rotariu, L.S.; Sytar, O.; Sestito, S.; Rapposelli, S.; Akram, M.; Iqbal, M.; Krishna, A.; et al. Chitosan Nanoparticles as a Promising Tool in Nanomedicine with Particular Emphasis on Oncological Treatment. *Cancer Cell Int.* **2021**, *21*, 1–21, doi:10.1186/s12935-021-02025-4.
10. Procedures, E. Controlled Synthesis of Camptothecin - Polylactide Conjugates And. **2010**, 111–121.
11. Li, Q.-Y.; Zu, Y.-G.; Shi, R.-Z.; Yao, L.-P. Review Camptothecin: Current Perspectives. *Curr. Med. Chem.* **2006**, *13*, 2021–2039, doi:10.2174/092986706777585004.
12. Hu, J.K.; Suh, H.W.; Qureshi, M.; Lewis, J.M.; Yaqoob, S.; Moscato, Z.M.; Griff, S.; Lee, A.K.; Yin, E.S.; Mark Saltzman, W.; et al. Nonsurgical Treatment of Skin Cancer with Local Delivery of Bioadhesive Nanoparticles. *Proc. Natl. Acad. Sci. U. S. A.* **2021**, *118*, 1–8, doi:10.1073/pnas.2020575118.
13. Zahn, D.; Weidner, A.; Saatchi, K.; Häfeli, U.O.; Dutz, S. Biodegradable Magnetic Microspheres for Drug Targeting, Temperature Controlled Drug Release, and Hyperthermia. *Curr. Dir. Biomed. Eng.* **2019**, *5*, 161–164, doi:10.1515/cdbme-2019-0041.
14. Bao, H.; Zhang, Q.; Yan, Z. The Impact of Camptothecin-Encapsulated Poly(Lactic-co</Em>-Glycolic Acid) Nanoparticles on the Activity of Cytochrome P450 in Vitro. *Int. J. Nanomedicine* **2019**, *Volume 14*, 383–391, doi:10.2147/IJN.S188984.
15. Fan, D.; Cao, Y.; Cao, M.; Wang, Y.; Cao, Y.; Gong, T. Nanomedicine in Cancer Therapy. *Signal Transduct. Target. Ther.* **2023**, *8*, doi:10.1038/s41392-023-01536-y.

16. Yao, Y.; Zhou, Y.; Liu, L.; Xu, Y.; Chen, Q.; Wang, Y.; Wu, S.; Deng, Y.; Zhang, J.; Shao, A. Nanoparticle-Based Drug Delivery in Cancer Therapy and Its Role in Overcoming Drug Resistance. *Front. Mol. Biosci.* **2020**, *7*, 1–14, doi:10.3389/fmolb.2020.00193.
17. Landgraf, M.; Lahr, C.A.; Kaur, I.; Shafiee, A.; Sanchez-Herrero, A.; Janowicz, P.W.; Ravichandran, A.; Howard, C.B.; Cifuentes-Rius, A.; McGovern, J.A.; et al. Targeted Camptothecin Delivery via Silicon Nanoparticles Reduces Breast Cancer Metastasis. *Biomaterials* **2020**, *240*, 119791, doi:10.1016/j.biomaterials.2020.119791.
18. Gustavson, D.E.; Miyake, A. Mesoporous Silica Nanoparticle Delivery of Chemically Modified SiRNA Against TWIST1 Leads to Reduced Tumor Burden. *Cogn. Emot. J.* **2016**, *30*, 1289–1303, doi:10.1016/j.nano.2015.05.011.
19. Sæbø, I.P.; Bjørås, M.; Franzyk, H.; Helgesen, E.; Booth, J.A. Optimization of the Hemolysis Assay for the Assessment of Cytotoxicity. *Int. J. Mol. Sci.* **2023**, *24*, doi:10.3390/ijms24032914.
20. Shakeran, Z.; Keyhanfar, M.; Varshosaz, J.; Sutherland, D.S. Biodegradable Nanocarriers Based on Chitosan-Modified Mesoporous Silica Nanoparticles for Delivery of Methotrexate for Application in Breast Cancer Treatment. *Mater. Sci. Eng. C* **2021**, *118*, 111526, doi:10.1016/j.msec.2020.111526.
21. Busey, R.H.; Mesmer, R.E. / E. **1977**, *16*, 2444–2450.
22. Guo, L.; Chen, H.; He, N.; Deng, Y. Effects of Surface Modifications on the Physicochemical Properties of Iron Oxide Nanoparticles and Their Performance as Anticancer Drug Carriers. *Chinese Chem. Lett.* **2018**, *29*, 1829–1833, doi:10.1016/j.cclet.2018.10.038.
23. Yoncheva, K.; Vandervoort, J.; Ludwig, A. Influence of Chitosan Layer on the Properties of Surface Modified Poly(Lactide-Co-Glycolide) Nanoparticles. *J. Dispers. Sci. Technol.* **2009**, *30*, 213–216, doi:10.1080/01932690802498666.
24. Shah, P. V.; Rajput, S.J. Facile Synthesis of Chitosan Capped Mesoporous Silica Nanoparticles: A PH Responsive Smart Delivery Platform for Raloxifene Hydrochloride. *AAPS PharmSciTech* **2018**, *19*, 1344–1357, doi:10.1208/s12249-017-0949-0.
25. Babaei, M.; Abnous, K.; Taghdisi, S.M.; Taghavi, S.; Sh. Saljooghi, A.; Ramezani, M.; Alibolandi, M. Targeted Rod-Shaped Mesoporous Silica Nanoparticles for the Co-Delivery of Camptothecin and Survivin ShRNA in to Colon Adenocarcinoma in Vitro and in Vivo. *Eur. J. Pharm. Biopharm.* **2020**, *156*, 84–96, doi:10.1016/j.ejpb.2020.08.026.
26. Buchman, J.T.; Elmer, W.H.; Ma, C.; Landy, K.M.; White, J.C.; Haynes, C.L. Chitosan-Coated Mesoporous Silica Nanoparticle Treatment of Citrullus Lanatus (Watermelon): Enhanced Fungal Disease Suppression and Modulated Expression of Stress-Related Genes. *ACS Sustain. Chem. Eng.* **2019**, *7*, 19649–19659, doi:10.1021/acssuschemeng.9b04800.
27. Popat, A.; Liu, J.; Lu, G.Q.; Qiao, S.Z. A PH-Responsive Drug Delivery System Based on Chitosan Coated Mesoporous Silica Nanoparticles. *J. Mater. Chem.* **2012**, *22*, 11173–11178, doi:10.1039/c2jm30501a.
28. Carrera Espinoza, M.J.; Lin, K.S.; Weng, M.T.; Kunene, S.C.; S.-S. Wang, S. In Vitro Studies of Pluronic F127 Coated Magnetic Silica Nanocarriers for Drug Delivery System Targeting Liver Cancer. *Eur. Polym. J.* **2021**, *153*, 110504, doi:10.1016/j.eurpolymj.2021.110504.
29. Jin, M.H.; Park, J.H.; Oh, D.; Park, J.S.; Lee, K.Y.; Lee, D.W. Effect of the Amine Group Content on Catalytic Activity and Stability of Mesoporous Silica Supported Pd Catalysts for Additive-Free Formic Acid Dehydrogenation at Room Temperature. *Int. J. Hydrogen Energy* **2019**, *44*, 4737–4744, doi:10.1016/j.ijhydene.2018.12.208.
30. Subramanian, N.; Sundaraganesan, N.; Sudha, S.; Aroulmoji, V.; Sockalingam, G.D.; Bergamin, M. Experimental and Theoretical Investigation of the Molecular and Electronic Structure of Anticancer Drug Camptothecin. *Spectrochim. Acta - Part A Mol. Biomol. Spectrosc.* **2011**, *78*, 1058–1067, doi:10.1016/j.saa.2010.12.049.
31. Jackson, N.; Ortiz, A.C.; Jerez, A.; Morales, J.; Arriagada, F. Kinetics and Mechanism of Camptothecin Release from Transferrin-Gated Mesoporous Silica Nanoparticles through a PH-Responsive Surface Linker. *Pharmaceutics* **2023**, *15*, doi:10.3390/pharmaceutics15061590.
32. Chen, G.; Mi, J.; Wu, X.; Luo, C.L.; Li, J.B.; Tang, Y.X.; Li, J. Structural Features and Bioactivities of the Chitosan. *Int. J. Biol. Macromol.* **2011**, *49*, 543–547, doi:10.1016/j.ijbiomac.2011.06.009.
33. Saini, K.; Bandyopadhyaya, R. Transferrin-Conjugated Polymer-Coated Mesoporous Silica Nanoparticles Loaded with Gemcitabine for Killing Pancreatic Cancer Cells. *ACS Appl. Nano Mater.* **2020**, *3*, 229–240, doi:10.1021/acsanm.9b01921.
34. Thahir, R.; Wahab, A.W.; Nafie, N. La; Raya, I. Synthesis of High Surface Area Mesoporous Silica SBA-15 by Adjusting Hydrothermal Treatment Time and the Amount of Polyvinyl Alcohol. *Open Chem.* **2019**, *17*, 963–971, doi:10.1515/chem-2019-0106.
35. Nairi, V.; Medda, S.; Piludu, M.; Casula, M.F.; Vallet-Regì, M.; Monduzzi, M.; Salis, A. Interactions between Bovine Serum Albumin and Mesoporous Silica Nanoparticles Functionalized with Biopolymers. *Chem. Eng. J.* **2018**, *340*, 42–50, doi:10.1016/j.cej.2018.01.011.

36. El-Hefian, E.A.; Nasef, M.M.; Yahaya, A.H. Preparation and Characterization of Chitosan/Agar Blended Films: Part 2. Thermal, Mechanical, and Surface Properties. *E-Journal Chem.* **2012**, *9*, 510–516, doi:10.1155/2012/285318.
37. Monsalve, Y.; Sierra, L.; López, B.L. Preparation and Characterization of Succinyl-Chitosan Nanoparticles for Drug Delivery. *Macromol. Symp.* **2015**, *354*, 91–98, doi:10.1002/masy.201400128.
38. Lu, J.; Liong, M.; Zink, J.I.; Tamanoi, F. Mesoporous Silica Nanoparticles as a Delivery System for Hydrophobic Anticancer Drugs. *Small* **2007**, *3*, 1341–1346, doi:10.1002/smll.200700005.
39. Llinàs, M.C.; Martínez-Edo, G.; Cascante, A.; Porcar, I.; Borrós, S.; Sánchez-García, D. Preparation of a Mesoporous Silica-Based Nano-Vehicle for Dual DOX/CPT Ph-Triggered Delivery. *Drug Deliv.* **2018**, *25*, 1137–1146, doi:10.1080/10717544.2018.1472678.
40. Zhang, X.; Lin, Y.; Gillies, R.J. Tumor PH and Its Measurement. *J. Nucl. Med.* **2010**, *51*, 1167–1170, doi:10.2967/jnumed.109.068981.
41. Lu, J.; Liong, M.; Zink, J.I.; Tamanoi, F. Mesoporous Silica Nanoparticles as a Delivery System for Hydrophobic Anticancer Drugs. *Small* 2007, *3*, 1341–1346.
42. Gan, Q.; Wang, T. Chitosan Nanoparticle as Protein Delivery Carrier-Systematic Examination of Fabrication Conditions for Efficient Loading and Release. *Colloids Surfaces B Biointerfaces* **2007**, *59*, 24–34, doi:10.1016/j.colsurfb.2007.04.009.
43. Botella, P.; Abasolo, I.; Fernández, Y.; Muniesa, C.; Miranda, S.; Quesada, M.; Ruiz, J.; Schwartz, S.; Corma, A. Surface-Modified Silica Nanoparticles for Tumor-Targeted Delivery of Camptothecin and Its Biological Evaluation. *J. Control. Release* **2011**, *156*, 246–257, doi:10.1016/j.jconrel.2011.06.039.
44. Huarte, J.; Espuelas, S.; Lai, Y.; He, B.; Tang, J.; Irache, J.M. Oral Delivery of Camptothecin Using Cyclodextrin/Poly(Anhydride) Nanoparticles. *Int. J. Pharm.* **2016**, *506*, 116–128, doi:10.1016/j.ijpharm.2016.04.045.
45. Fu, C.; Qin, J.; Liu, X.; Kong, F. Galactosed and Reduction-Responsive Nanoparticles Assembled from Trimethylchitosan–Camptothecin Conjugates for Enhanced Hepatocellular Carcinoma Therapy. *Pharmaceutics* **2022**, *14*, doi:10.3390/pharmaceutics14071315.
46. Ye, Y.; Hu, X. A PH-Sensitive Injectable Nanoparticle Composite Hydrogel for Anticancer Drug Delivery. *J. Nanomater.* **2016**, *2016*, doi:10.1155/2016/9816461.
47. Abedi, M.; Abolmaali, S.S.; Abedanzadeh, M.; Farjadian, F.; Samani, S.M.; Tamaddon, A.M. Core–Shell Imidazoline–Functionalized Mesoporous Silica Superparamagnetic Hybrid Nanoparticles as a Potential Theranostic Agent for Controlled Delivery of Platinum(II) Compound. *Int. J. Nanomedicine* **2020**, *15*, 2617–2631, doi:10.2147/IJN.S245135.
48. Hu, B.; Wang, J.; Li, J.; Li, S.; Li, H. Superiority of L-Tartaric Acid Modified Chiral Mesoporous Silica Nanoparticle as a Drug Carrier: Structure, Wettability, Degradation, Bio-Adhesion and Biocompatibility. *Int. J. Nanomedicine* **2020**, *15*, 601–618, doi:10.2147/IJN.S233740.
49. Harpe, K.; Kondiah, P.; Choonara, Y.; Marimuthu, T.; Toit, L.; Pillay, V. The Hemocompatibility of Nanoparticles : A Review. *Cells* **2019**, *8*, 1–25.
50. Yedgar, S.; Barshtein, G.; Gural, A. Hemolytic Activity of Nanoparticles as a Marker of Their Hemocompatibility. *Micromachines* **2022**, *13*, 1–15, doi:10.3390/mi13122091.